Int. J. Heat Mass Transfer. Vol. 30, No. 2, pp. 351–361, 1987
Printed in Great Britain

0017–9310/87 $3.00 + 0.00
Pergamon Journals Ltd.

Stability of a free convection density-extremum flow in a porous medium

SUNIL KUMAR* and NICHOLAS D. KAZARINOFF

Department of Mathematics, State University of New York, Buffalo, NY 14214, U.S.A.

(*Received* 13 *December* 1984 *and in final form* 10 *June* 1986)

Abstract—The relative stability of the multiple steady states of laminar free convection flows in a porous medium saturated with cold, pure water along a vertical, isothermal, planar surface is investigated. Two distinct regions of numerically computed multiple steady-state solutions for flow conditions in which the internal temperature range spans a density maximum ($0 < R < 1/2$, where R is a temperature ratio parameter) have been reported in the literature. Stability analysis of these steady states is performed by linearizing the time-dependent equations about the steady-state solutions and by considering only amplification or decay of perturbations with time. The results obtained indicate that all but one of the multiple steady states at each R are unstable with respect to time. Relative merits and demerits of the approach used in this study over the conventional hydrodynamic stability analysis are discussed.

1. INTRODUCTION

FLUID motion in natural convection processes arises from the differences in density of the fluid which are caused by the variation of temperature across the flow field. Reversals of the resulting buoyancy force may occur if the internal temperature range of the flow field contains the temperature at which the density of the fluid attains a maximum value. This leads to complex convective effects, such as reversals in the flow and nonsteady flow.

In this study, the system under consideration is a vertical, planar, isothermal surface adjacent to quiescent, cold, pure water saturating a porous medium. Such flows are found in the melting and freezing of ice surfaces, in process technology, and near cold rock faces against saturated sand beds. In the region adjoining the vertical surface, the temperature variations considered span the temperature at which the maximum density occurs, see Figs. 1 and 2. (The density of pure water at atmospheric pressure is maximum at about 4°C.) The resulting multiple steady-state flows (which are numerically obtained [1]) are then examined for their stability. The conventional method of analysis of hydrodynamic stability is not invoked, but a linearized stability analysis of the steady states, considering only amplification or decay with time, is made.

The different approach adopted in this study is to derive the linear stability equations from a purely mathematical standpoint and to examine the stability of the steady state solutions in the same spirit, i.e. by following as closely as possible the classical analysis which studies stability of solutions of

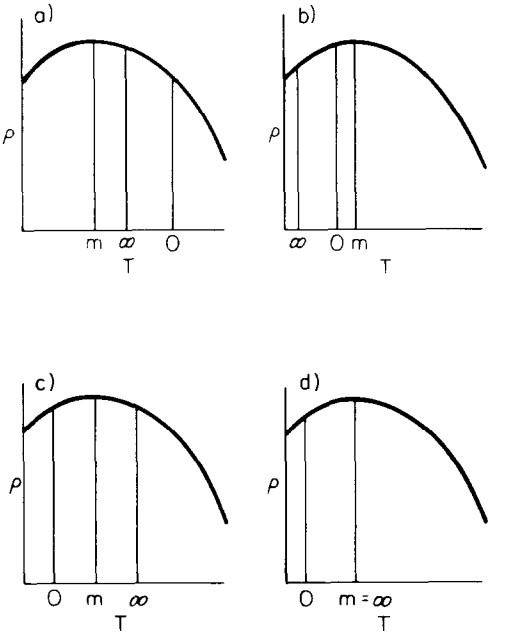

FIG. 1. Qualitative sketch of water density vs temperature: (a) $R < 0$ upflow; (b) $R > 1$ downflow; (c) $R \simeq 0.5$ downflow; (d) $R = 0$ upflow.

$\partial \mathbf{F}(\eta, \tau)/\partial \tau = L\mathbf{F}(\eta, \tau)$ by introducing $\mathbf{F}(\eta, \tau) = \mathbf{f}(\eta)\exp(\lambda\tau)$ (where L is a linear operator in η). It is the final transformed equations whose mathematical stability is studied, instead of the original equations of rates of change of momentum and energy. However, as demonstrated in the Appendix, the results obtained can be interpreted to be the asymptotic limit of the traditional hydrodynamic case when the perturbations allowed are real valued (the zero frequency limit) and the wave number goes to zero as well. The principal disadvantage of the approach used here is that less information is obtained about the physics of

* Current address: Department of Mechanical Engineering, University of California, Berkeley, CA 94720, U.S.A.

NOMENCLATURE

a	complex number used as exponent in the perturbations considered in the Appendix, equations (A5)
$A(z)$	ancillary function on the unit interval, equation (27)
$B(z)$	ancillary function on the unit interval, equation (27)
c	constant, equations (18) and (21)
c_1	constant, equation (10)
$c*$	constant, equation (21)
C_p	specific heat
$D(z)$	ancillary function on the unit interval, equation (27)
$E(z)$	ancillary steady-state temperature gradient on the unit interval, equation (14)
$f(\eta, \tau)$	similarity streamfunction
g	acceleration due to gravity
$H(z)$	ancillary steady-state streamfunction on the unit interval, equation (14)
k	thermal conductivity
K	permeability of the median
$p(x, y, t)$	pressure
q	exponent in the density relation, equation (2)
R	temperature ratio parameter, equation (1)
Ra_x	local Rayleigh number, equation (10)
t	time
$T(x, y, t)$	temperature
$u(x, y, z)$	Darcy velocity in the x direction $(= \partial\psi/\partial y)$
$v(x, y, t)$	Darcy velocity in the y direction $(= -\partial\psi/\partial x)$
$\mathbf{V}(x, y, t)$	velocity vector with components u and v
x	coordinate along the vertical surface
y	coordinate perpendicular to the vertical surface
z	independent variable on the unit interval, equation (14).

Greek symbols

α	coefficient in the density relation, equation (2)
α_1	thermal diffusivity, equation (6)
β	complex number used as exponent in the perturbations in Appendix, equation (A5)
$\beta*$	complex number, equation (A7)
δ	small number close to zero, Section 3
ε	small value for linearizing
η	similarity variable, equation (9)
λ	eigenvalue
μ	viscosity of the fluid
ρ	density
σ	porosity of the medium
τ	dimensionless time
$\phi(\eta, \tau)$	nondimensionalised temperature
$\psi(x, y, t)$	streamfunction $(u = \partial\psi/\partial y, v = -\partial\psi/\partial x)$.

Subscripts

e	effective
f	of the fluid
m	at the extremum condition
r	reference value
s	of the solid
0	at the wall
∞	at ambient condition.

Other symbols

$\bar{}$	steady-state value
$\hat{}$	perturbations of the steady-state
$\tilde{}$	eigenvectors associated with the particular form of perturbations considered.

the disturbed flow than if the traditional approach were successfully implemented, and information on downstream, selective frequency growth of amplitude is lost.

This approach is selected over the conventional one because of the following considerations. As demonstrated in the Appendix, the traditional approach of studying hydrodynamic stability leads to a singularity in the stability equations if a nonlinear variation of density with temperature (of the specific mathematical form indicated in Section 2) is assumed. However, the presence of this singularity is not very serious since it can be avoided by making additional assumptions (see the Appendix). But the resulting system of equations is still quite complicated, and even after suitable similarity transformations contains the x (vertical) coordinate in the coefficients in a nontrivial way. Further, the system is of sixth order. Since we are investigating two entire families of multiple steady-state solutions to indicate which of them are stable, and not just the stability curves corresponding to a single steady-state solution (for example, as is done

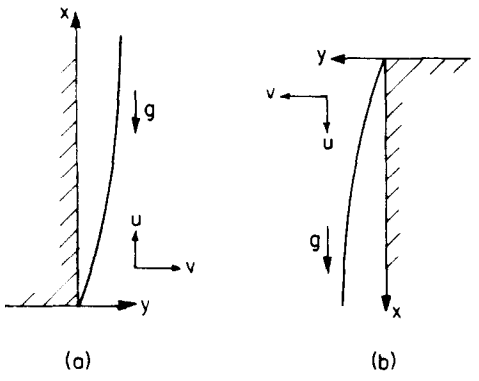

FIG. 2. Coordinate system: (a) upflow (R near 0); (b) downflow (R near 0.5).

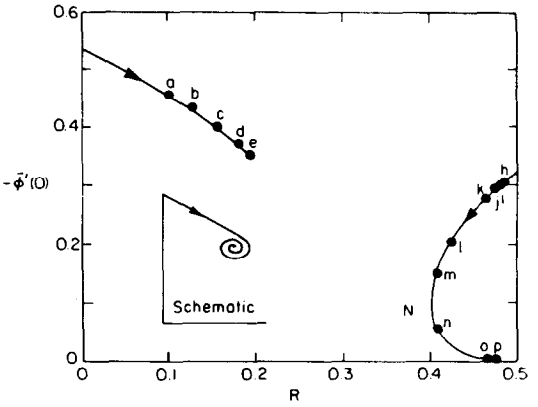

FIG. 3. Bifurcation diagram of the steady state in terms of $\bar{\phi}(0)$.

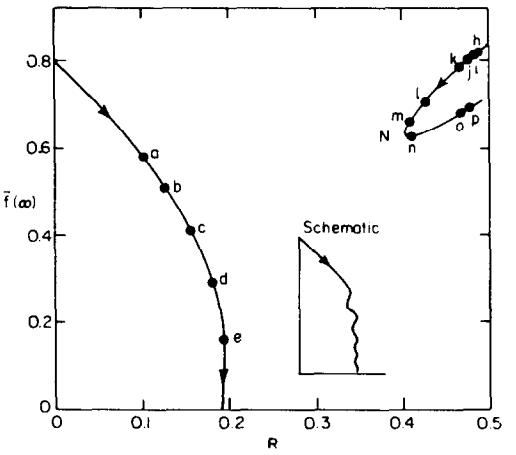

FIG. 4. Bifurcation diagram of the steady state in terms of $\bar{f}(\infty)$.

in refs. [2, 3] for systems in nonporous environments), implementation of the classical approach would require a major computational effort.

The approach adopted yields a simpler system of equations which leads to a determination of the relative stability of the various steady-state solutions, and significant results are obtained with a saving of much effort. The linear system of equations obtained are of third order and have a less complicated x dependence in the coefficients as compared to the x dependence in the equations that result from the classical formulation. Moreover, the boundary value problem for the stability equations in this study is also transformed from a problem on a semi-infinite interval to one of the unit interval. This saves computational resources; and, more importantly, enables the computation of eigenvalues and eigenvectors which could not be found through computations on the original semi-infinite interval.

Two families of steady-state solutions, one for R near and greater than 0, and the second for R near and less than 0.5 (where R is a temperature ratio parameter, see Nomenclature) are computed. For values of R between these two ranges no steady-state solutions (as reported by Gebhart *et al.* [1]) have been found. The second family (R near 0.5) has two steady-state solutions at each value of R and the corresponding bifurcation diagram has only one nose (point of vertical tangency, see Figs. 3 and 4). For this family only one eigenvalue λ was found. It changes sign at the nose, indicating that only one of the two steady-state solutions at each R may be stable with respect to time while the other certainty is unstable. For the first family of solutions (near $R = 0$, see Figs. 3–5), the bifurcation diagram for the steady states has many noses, three of which have been numerically obtained, and many more are conjectured [1, 4, 5]. Many eigenvalues have been computed, all of which are negative for the range of R over which a single solution exists, and for the continuation of this range to the first nose of the bifurcation diagram. Also the ith eigenvalue ($i = 1, 2$) changes sign from negative to positive at the ith nose of the bifurcation diagram and then remains positive. The third and the further eigenvalues could not be numerically continued past the first nose (because of difficulties described in Section 3). Thus the flows corresponding to solutions in the single-solution range of R continued to the first nose may be stable, and the flows corresponding to other steady-state solutions in the multiple-solution range of R are only conditionally stable, becoming more unstable as we continue down the bifurcation curve.

The results of the stability analysis establish that all heat transfer coefficients but one are unstable at each R, and thus preclude any possibility of harnessing in technology the multiple heat rates that are numerically predicted. For analogous results, see refs. [6, 7].

Similar bifurcation has been observed for the same flow configuration in a nonporous environment [8]. (See refs. [6–8] for a comprehensive list of related experimental and theoretical studies.) A conventional stability analysis for this case has been performed by Hwang [7], and neutral stability curves have been

obtained. By implementing the present analysis to the same problem [6], results that are qualitatively similar to those in ref. [7] are observed. Thus the present method (which is simpler and requires less computational effort than the traditional method, and yields qualitatively similar conclusions) is relatively superior and can be introduced as a general stability theory in heat and mass transfer for problems that exhibit bifurcation in the steady state, and where the bifurcation curve contains at least one point of vertical tangency. Examples of such can be found in refs. [1, 4–9].

2. MATHEMATICAL FORMULATION

The vertical, isothermal surface is assumed at constant temperature T_0 and is adjacent to quiescent cold water saturating a porous medium at an ambient temperature of T_∞. This temperature range is assumed to be close to temperature T_m ($\simeq 4°C$) at which the density extremum occurs, see Fig. 1. The parameter that characterizes the temperatures in the system, and their relative positions and magnitudes is R which is defined as [1, 10]

$$R = (T_m - T_\infty)/(T_0 - T_\infty). \tag{1}$$

A buoyancy force reversal arises for $0 < R < 1/2$ [1] which lies in the inner portion of the thermal region (close to surface) for R somewhat less than 1/2, and in the outer portion for R close to 0. From Fig. 2 it may be observed that the flow is upward for $R < 0$ and downward for $R > 1/2$.

When fluid flows slowly through permeable material, motion is resisted according to Darcy's law [11–14], which states that the hydraulic gradient is proportional to the fluid velocity and to its viscosity, and is inversely proportional to the permeability. In the equations of motion for creeping flow, the Darcy resistance term replaces the Navier–Stokes viscosity term. Using the Boussinesq approximation and the density relationship for cold water [15]:

$$\rho_f = \rho_{mf}[1 - \alpha|T - T_m|^q] \tag{2}$$

the equations governing the velocity and temperature fields are [12–14]:

$$\nabla \cdot \mathbf{V} = 0 \tag{3a}$$

$$\frac{\rho_{fr}}{\sigma}\frac{\partial \mathbf{V}}{\partial t} + \frac{\mu_r}{K}\mathbf{V} = -\nabla p + \rho_{mf}[1 - \alpha|T - T_m|^q]\mathbf{g} \tag{3b}$$

$$(\rho C_p)_{er}\frac{\partial T}{\partial t} + (\rho C_p)_{fr}\mathbf{V}\cdot\nabla T = k_{er}\nabla^2 T \tag{3c}$$

where [13]

$$(\rho C_p)_e = (1 - \sigma)(\rho C_p)_s + \sigma(\rho C_p)_f,$$
$$k_e = (1 - \sigma)k_s + \sigma k_f. \tag{4}$$

It is assumed that in equations (3), $\mathbf{V}$ and T are the only variables and the other coefficients are constant. Hence a subscript r has been added to denote constant reference quantities.

The hypotheses that were made to arrive at above equations are [10]: the saturating liquid and the porous medium are in local thermodynamic equilibrium; the physical properties of the fluid and the medium are isotropic and homogeneous; and the empirical Darcy's law is valid.

The appropriate boundary conditions for the two-dimensional system under study are

$$\mathbf{V}(x,0,t) = \mathbf{V}(x,\infty,t) = T(x,0,t) - T_0$$
$$= T(x,\infty,t) - T_\infty$$
$$= 0. \tag{5}$$

The equations governing steady-state, natural convection can be extracted from equations (3) by deleting the time derivative. Defining

$$\alpha_1 = k_{er}/(\rho C_p)_{fr}, \tag{6}$$

and following the analysis presented in ref. [10], the pressure terms in equation (3b) are eliminated through cross differentiation. The boundary-layer approximations are then applied, which result in neglecting the change in $\bar{v}$ with respect to x, as compared to $\bar{u}$ with respect to y. Conduction in the direction of the flow is also neglected. Integrating the resulting velocity equation and applying the boundary condition at ∞ [equation (5)] results in [10]

$$\bar{u}(x,y) = \pm\frac{K}{\mu_r} g\,\alpha\rho_{mf}[|\bar{T} - T_m|^q - |T_\infty - T_m|^q] \tag{7a}$$

$$\bar{u}\frac{\partial \bar{T}}{\partial x} + \bar{v}\frac{\partial \bar{T}}{\partial y} = \alpha_1\frac{\partial^2 \bar{T}}{\partial y^2} \tag{7b}$$

where $0 \leqslant y \leqslant \infty$, $0 \leqslant x \leqslant \infty$, and

$$\bar{u}(x,0) = \bar{v}(x,0) = \bar{u}(x,\infty) = \bar{v}(x,\infty) = 0 \tag{8a}$$

$$\bar{T}(x,0) - T_0 = \bar{T}(x,\infty) - T_\infty = 0. \tag{8b}$$

The plus sign in equation (7a) corresponds to the coordinate system in Fig. 2a and the minus sign to that in Fig. 2b.

A similarity variable is defined as [10]

$$\eta = \frac{y}{2x}(Ra_x)^{1/2} \tag{9}$$

where Ra_x is the local Rayleigh number and is defined as

$$Ra_x = c_1^2 x,$$
$$c_1^2 = 2K\alpha\rho_{mf}g|T_0 - T_\infty|^q/(\mu_r\alpha_1). \tag{10}$$

A normalised, steady-state temperature $\bar{\phi}(\eta)$ and a similarity, steady-state streamfunction $\bar{f}(\eta)$ are defined as [1, 10]

$$\bar{\phi}(\eta) = [\bar{T}(x,y) - T_\infty]/(T_0 - T_\infty),$$
$$\bar{f}(\eta) = \bar{\psi}(x,y)/[\alpha_1(Ra_x)^{1/2}]. \tag{11}$$

From equations (9)–(11), and the definition of the

streamfunction $\bar{\psi}$ (see Nomenclature), the steady-state equations (7) become (for $0 \leqslant \eta \leqslant \infty$)

$$\frac{d\bar{f}}{d\eta} = \pm[|\bar{\phi} - R|^q - |R|^q],$$

$$\frac{d^2\bar{\phi}}{d\eta^2} + \bar{f}\frac{d\bar{\phi}}{d\eta} = 0. \tag{12}$$

The plus/minus signs correspond to Figs. 2a/2b, respectively. The corresponding boundary conditions are

$$\bar{f}(0) = \bar{\phi}(0) - 1 = \bar{\phi}(\infty) = 0. \tag{13}$$

It has been shown [1] that $\bar{\phi}(\eta)$ is strictly decreasing for $\eta \geqslant 0$ and can be taken as an independent variable. Thus letting [1]

$$z = \bar{\phi}(\eta), \qquad E(z) = -\frac{d\bar{\phi}(\eta)}{d\eta},$$

$$H(z) = \bar{f}(\eta) \tag{14}$$

equations (12) become (for $0 \leqslant z \leqslant 1$)

$$\frac{dH(z)}{dz} = \mp\frac{(|z - R|^q - |R|^q)}{E(z)},$$

$$\frac{dE(z)}{dz} = H(z). \tag{15}$$

The minus/plus sign in equation (15) corresponds to the coordinate system in Figs. 2a/2b, respectively. The corresponding boundary conditions are

$$H(1) = E(0) = 0. \tag{16}$$

The change in variables thus converts the autonomous, third-order, boundary-value problem on the semi-infinite interval, given by equations (12) and (13), to the nonautonomous, second-order, two-point boundary-value problem on the unit interval, as given by equations (15) and (16).

Following the analysis used to obtain equations (7), the time-dependent equations (3b, c) are simplified to obtain

$$\frac{K\rho_{fr}}{\sigma\mu_r}\frac{\partial u}{\partial t} + u = \pm\frac{K\alpha\rho_{mf}g}{\mu_r}[|T - T_m|^q - |T_\infty - T_m|^q] \tag{17a}$$

$$\frac{(\rho C_p)_{er}}{(\rho C_p)_{fr}}\frac{\partial T}{\partial t} + u\frac{\partial T}{\partial x} + v\frac{\partial T}{\partial y} = \alpha_1\frac{\partial^2 T}{\partial y^2} \tag{17b}$$

The corresponding boundary conditions are expressed by equation (5).

A scaled time is then defined as

$$\tau = ct \tag{18}$$

where c is a constant to be determined for convenience. Using the similarity variable η defined by equation (9), a normalized temperature and similarity streamfunction [based on equation (11)] are introduced as

$$\phi(\eta, \tau) = \frac{T(x, y, t) - T_\infty}{T_0 - T_\infty},$$

$$f(\eta, \tau) = \frac{\psi(x, y, t)}{\alpha_1(Ra_x)^{1/2}}. \tag{19}$$

Using equations (9), (10), (18), (19), the following is obtained from equations (17) (for $0 \leqslant \eta \leqslant \infty$)

$$\frac{\partial^2 f}{\partial\eta\partial\tau} + \frac{\partial f}{\partial\eta} = \pm[|\phi - R|^q - |R|^q],$$

$$c^* x\frac{\partial\phi}{\partial\tau} - f\frac{\partial\phi}{\partial\eta} = \frac{\partial^2\phi}{\partial\eta^2}. \tag{20}$$

As before, the plus/minus signs correspond to Figs. 2a/2b, respectively. Also, c (chosen to nondimensionalize τ) and c^* are

$$c = \frac{\sigma\mu_r}{K\rho_{fr}}, \qquad c^* = \frac{(\rho C_p)_{er}}{(\rho C_p)_{fr}}\frac{4}{(\alpha_1 c_1^2)}\frac{\sigma\mu_r}{(K\rho_{fr})}. \tag{21}$$

The boundary conditions are

$$f(0, \tau) = \phi(0, \tau) - 1 = \phi(\infty, \tau) = 0. \tag{22}$$

Stability analysis

The nonlinear τ-dependent equations (20) are linearized about the steady-state solutions $\bar{f}(\eta)$ and $\bar{\phi}(\eta)$, whose stability is under consideration. This is achieved by considering solutions of the form

$$f(\eta, \tau) = \bar{f}(\eta) + \varepsilon\hat{f}(\eta, \tau) + O(\varepsilon^2), \tag{23a}$$

$$\phi(\eta, \tau) = \bar{\phi}(\eta) + \varepsilon\hat{\phi}(\eta, \tau) + O(\varepsilon^2) \tag{23b}$$

where $\hat{f}(\eta, \tau)$ and $\hat{\phi}(\eta, \tau)$ are perturbations of $\bar{f}$ and $\bar{\phi}$, respectively, and ε is small and positive. Substituting equations (23) into equations (20), and using equations (12) to 'cancel out' the base flow (steady-state) terms, a system of partial differential equations is obtained (after dividing through by ε and taking limits as ε tends to zero) in which the time derivative $\partial/\partial\tau$ appears in the equations governing $\hat{f}$ (as it should), but in the equation for $\hat{\phi}$ it appears as part of $\partial^2/\partial\eta\partial\tau$. Thus the system is not of the usual form, $\partial V/\partial\tau = L_\eta V$ (L_η is a linear operator), for a linear stability analysis to be rigorously carried out. However, the following analysis proceeds as if the system were susceptible to the usual linear stability analysis.

The perturbations $\hat{f}$ and $\hat{\phi}$ are assumed to be of the form

$$\hat{f}(\eta, \tau) = e^{\lambda\tau}\tilde{f}(\eta), \qquad \hat{\phi}(\eta, \tau) = e^{\lambda\tau}\tilde{\phi}(\eta). \tag{24}$$

Substituting equations (23) and (24) into equations (20), cancelling out the steady state [equations (12)], and taking the limit as ε goes to zero yields (for $0 \leqslant \eta \leqslant \infty$)

$$[\lambda + 1]\frac{d\tilde{f}}{d\eta} = \pm q\,\mathrm{sign}(\bar{\phi} - R)|\bar{\phi} - R|^{q-1}\tilde{\phi}. \tag{25a}$$

$$c^* x\lambda\tilde{\phi} - \left[\bar{f}\frac{d\tilde{\phi}}{d\eta} + \tilde{f}\frac{d\bar{\phi}}{d\eta}\right] = \frac{d^2\tilde{\phi}}{d\eta^2}. \tag{25b}$$

Again, the plus/minus signs correspond to Figs. 2a/2b, respectively. The corresponding boundary conditions are

$$\bar{f}(0) = \bar{\phi}(0) = \bar{\phi}(\infty) = 0. \tag{26}$$

Equations (25) and (26) form an eigenvalue problem if we assign particular numerical value to x.

A transformation of equations (25) and (26) to a unit interval is achieved by using z [defined by equation (14)] as an independent variable and by defining

$$A(z) = \bar{f}(\eta), \qquad B(z) = \bar{\phi}(\eta),$$
$$D(z) = -\frac{\mathrm{d}\bar{\phi}(\eta)}{\mathrm{d}\eta}. \tag{27}$$

Using equations (14) and (27), equations (25) yield (for $0 \leqslant z \leqslant 1$)

$$\frac{\mathrm{d}A(z)}{\mathrm{d}z} = \frac{\mp q \,\mathrm{sign}\,(z - R)|z - R|^{q-1}}{(\lambda + 1)E(z)} B(z) \tag{28a}$$

$$\frac{\mathrm{d}B(z)}{\mathrm{d}z} = \frac{D(z)}{E(z)} \tag{28b}$$

$$\frac{\mathrm{d}D(z)}{\mathrm{d}z} = c^* x\lambda \frac{B(z)}{E(z)} + H(z)\frac{D(z)}{E(z)} + A(z). \tag{28c}$$

The boundary conditions are obtained from equations (27) and (14) as

$$A(1) = B(0) = B(1) = 0. \tag{29}$$

The minus/plus signs in equation (28a) correspond to the coordinate systems in Figs. 2a/2b, respectively.

The change in variable enables the eigenvalue problem on the semi-infinite interval [equations (25)] to be converted to that on a unit interval. Of course, a specific numerical value must be assigned to x for the problem to be well-posed.

3. NUMERICAL RESULTS AND DISCUSSION

Equations (25) and (26) are solved by choosing λ as an additional unknown and by appending the trivial differential equation

$$\frac{\mathrm{d}\lambda}{\mathrm{d}\eta} = 0. \tag{30}$$

An additional normalizing boundary condition is specified as

$$\bar{f}(\infty) = 1, \qquad \text{for } R \textit{ near} \text{ and } > 0 \tag{31a}$$

$$\frac{\mathrm{d}\bar{\phi}(0)}{\mathrm{d}\eta} = 1, \qquad \text{for } R \textit{ near} \text{ and } < 0.5. \tag{31b}$$

The eigenvalue problem thus obtained is solved on a finite interval $[0, \eta_\infty]$ with the boundary condition at ∞ imposed at η_∞. The same fixed value of η_∞ was not used at every R, but instead η_∞ was so chosen that both the steady-state solutions as well as the eigenvectors converged smoothly and exponentially to their respective conditions at ∞. It is observed that if η_∞ is chosen to be much greater than the smallest such value, the eigenvectors exhibit some numerical instability manifested by slow decay and random small oscillations of their components at large η.

For the corresponding problem on the unit interval, given by equations (28) and (29), the eigenvalue problem is solved by appending equation (30) (with the derivative taken with respect to z), and considering boundary conditions [from equations (31) and (27)] of the form

$$A(0) = 1, \qquad \text{for } R \textit{ near} \text{ and } > 0 \tag{32a}$$

$$D(1) = -1, \qquad \text{for } R \textit{ near} \text{ and } < 0.5. \tag{32b}$$

In the range of R near to and less than 0.5, the family of steady-state solutions and the corresponding eigenvalues and eigenvectors are computed for the interval $[0, \eta_\infty]$. The values of η_∞ required were not large (no greater than 52). However, for R near to and greater than 0 very large values of η_∞ are required (typically 100 and greater) for the components of the solution to smoothly and exponentially reach their respective values at ∞, especially for small values of $\bar{f}(\infty)$. Thus equations (28) and (29) are used, which are equations for the unit interval. The problem of selecting a suitable η_∞ is then avoided and so are the errors involved in integrating over large intervals. Also by solving the problem on a unit interval enables the computation of eigenvalues and corresponding eigenvectors which would not have been found through computations on the original system.

Even so, it was observed that integrating near zero was quite difficult and equations (28) and (29) had to be solved on an interval $[1, \delta]$, where $\delta \to 0$ and the boundary conditions at δ are obtained from equations (28) and (29), and (32) by Taylor series expansion about 0. These boundary conditions are expressed as

$$A(\delta) = 1 - \frac{qR^{q-1}}{c^* x\lambda(\lambda + 1)}\delta,$$
$$B(\delta) = -\frac{H(0)}{c^* x\lambda}\delta \tag{33}$$

for R near and greater than 0. An integration from 0 to 1 (instead of from 1 to 0), by using the Taylor series expansion about 0 to obtain good guesses for the solution components near 0, could not be implemented because the coefficients in the Taylor series contain the value of λ [see equation (33)] which is unknown (and usually very small), thus making the coefficients of the Taylor expansion too sensitive to the guess of λ to be used.

Two different computer codes were used to obtain the numerical results: BOUNDS and COLSYS. BOUNDS is a two-point, boundary-value-problem solving routine that uses multiple shooting techniques [16–18], while COLSYS uses the method of collocation with B-splines [19]. The steady-state solution was first obtained by solving equations (12) and

(13) with BOUNDS. Since the solution provided by BOUNDS consists only of component values at a set of pre-determined mesh points, the solution was given to COLSYS to generate splines corresponding to components of the steady-state solution vector. These were then used by BOUNDS while solving the stability equations [equations (25) and (26)]. A similar approach was used while solving on the unit interval [equations (15) and (16), and (28) and (29), respectively]. The computations were performed on a CDC Cyber 174/730 computer system, and both BOUNDS and COLSYS were compiled by the FORTRAN 5 (FORTRAN 77) compiler under OPT = 2. Approximate run time for obtaining the steady-state solutions ranged from a few CPU seconds to about 30 s (for large η_∞), and for solving the linear stability equations for the CPU time was about 50 s for the range of R near 0, and about 150 s for the range of R near 0.5. The computations were carried out to an error less than 10^{-6}.

Before presenting the results we clarify what is meant by stable. By the statement that a steady state is stable we mean that small perturbations of the form specified by equation (24) decay exponentially to 0 as $t \to +\infty$ for each fixed (x, y). Similarly, unstable means that the absolute value of the perturbations grows exponentially to ∞ as $t \to +\infty$ for almost all fixed (x, y).

All computations were carried out for $q = 1.894816$, which corresponds to that for pure water at atmospheric pressure, see [15]. For the first family of solutions (R near 0, see Figs. 3–5 for bifurcation curves of the steady-state solution) nine eigenvalues and corresponding eigenvectors were found, see Tables 1 and 2 and Figs. 6 and 7. All the eigenvalues are negative in the single solution range continued to the first nose (point of vertical tangency) N_1 of the bifurcation diagram. The first eigenvalue changes sign from negative to positive at the first nose and remains positive thereafter. Similarly the second eigenvalue changes algebraic sign and becomes positive at the second nose N_2.

The third and further eigenvalues could not be computed past the first nose due to difficulties that were encountered. While numerically continuing the third and further eigenvalues and the corresponding eigenvectors past the first nose N_1, the computations would converge to the first and second eigenvalues and their corresponding eigenvectors (especially the second), rather than yielding the corresponding third and further eigenvalues and eigenvectors. All the eigenvalues λ_i are small negative numbers before and after the first nose N_1 (except λ_1 which becomes positive after the nose, but is small in magnitude); see Tables 1 and 2, and Figs. 6 and 7. The eigenvectors corresponding to different λ_i become almost identical as the first nose N_1 is approached from the single-solution range of R on the bifurcation diagram. We conjecture that just before the first nose N_1 the values

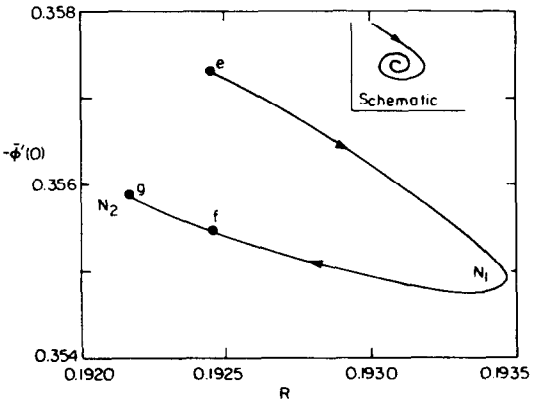

FIG. 5. A blown-up version of the bifurcation diagram in Fig. 3.

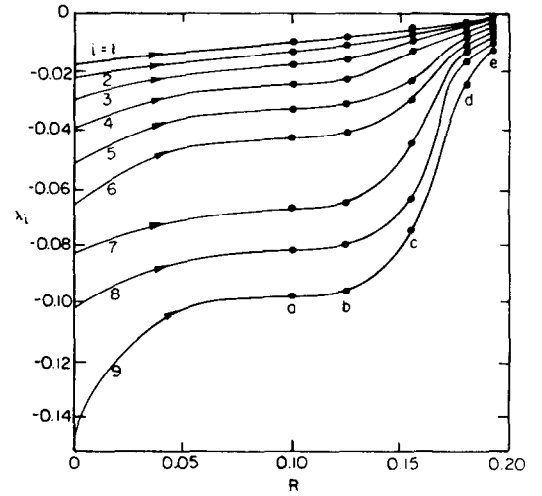

FIG. 6. The multiple eigenvalues λ_i for the family of solutions near $R = 0$.

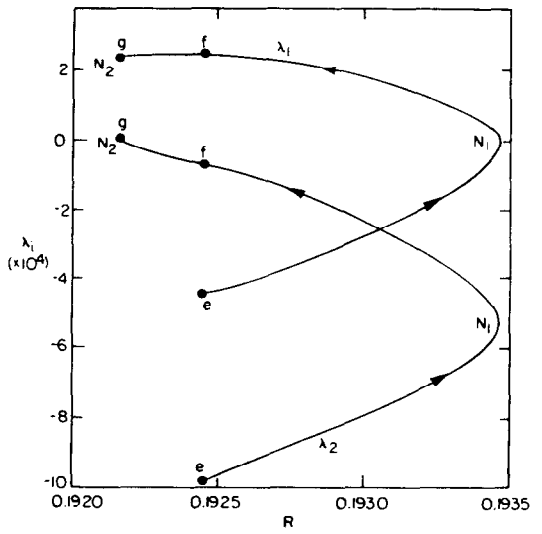

FIG. 7. A blown-up version of Fig. 6, showing the first two eigenvalues past the first and second noses.

Table 1. The first two eigenvalues for the family of solutions near $R = 0$

R	$\bar{f}(\infty)$	λ_1	λ_2	η_∞
0.000000	0.794702	-0.17337×10^{-1}	-0.21861×10^{-1}	28
0.050000	0.696221	-0.13123×10^{-1}	-0.16107×10^{-1}	34
0.100000	0.579459	0.93674×10^{-2}	-0.12330×10^{-1}	34 a‡
0.125000	0.510158	-0.74365×10^{-2}	-0.15318×10^{-1}	34 b
0.155000	0.408813	-0.46009×10^{-2}	-0.61153×10^{-2}	46 c
0.180000	0.287461	-0.21409×10^{-2}	-0.27418×10^{-2}	70 d
0.189296	0.210000	-0.10152×10^{-2}	-0.15234×10^{-2}	82
0.192446	0.160000	-0.44028×10^{-3}	-0.98621×10^{-3}	88 e
0.192813	0.150000	-0.34130×10^{-3}	-0.85313×10^{-3}	94
0.192655	0.050000	0.23579×10^{-3}	-0.10795×10^{-3}	†
0.192454	0.040000	0.24629×10^{-3}	-0.67733×10^{-4}	† f
0.192163	0.015000	0.24058×10^{-3}	-0.27318×10^{-5}	†
0.1921593	0.011750	0.23859×10^{-3}	-0.16631×10^{-6}	†
0.192160	0.010000	0.23762×10^{-3}	0.97532×10^{-6}	†
0.192164	0.007500	0.23640×10^{-3}	0.22748×10^{-5}	† g

† Computed on the unit interval.
‡ This point $[R, \bar{f}(\infty)]$ is identified on the plots by this alphabet. (All computations done at $c^*x = 10$.)

Table 2. The single eigenvalue for the family of solutions near $R = 0.5$

R	$-\bar{\phi}'(0)$	λ	η_∞
0.485000	0.308756	-0.23679×10^{-1}	28 h†
0.480000	0.301769	-0.23340×10^{-1}	28 i
0.475000	0.294583	-0.22994×10^{-1}	28 j
0.465000	0.279528	-0.22259×10^{-1}	28 k
0.425000	0.204477	-0.15482×10^{-1}	34 l
0.407125	0.150000	-0.74774×10^{-2}	34 m
0.400825	0.100000	-0.19839×10^{-3}	40
0.400820	0.098000	0.63129×10^{-4}	40
0.404360	0.065000	0.43707×10^{-2}	40
0.405613	0.060000	0.49576×10^{-2}	40
0.407107	0.055000	0.55221×10^{-2}	40 n
0.420000	0.0292305	0.78838×10^{-2}	40
0.440000	0.0107516	0.82761×10^{-2}	40
0.460000	0.0025985	0.68274×10^{-2}	46
0.465000	0.0015545	0.62415×10^{-2}	52 o
0.475000	0.0003492	0.48036×10^{-2}	52 p
0.480000	0.0001018	0.39475×10^{-2}	52
0.485000	0.0000132	0.30064×10^{-2}	52

† This point $[R, \bar{\phi}'(0)]$ is identified on the graph by this alphabet. (All computations done at $c^*x = 10$.)

of $\lambda_3, \lambda_4, \ldots$ are closer to the values of λ_1 and λ_2 just after this nose. Thus our numerical computations jump from $\lambda_3, \lambda_4, \ldots$ to the values of λ_1 and λ_2 as one passes beyond N_1. To avoid this, guesses based on the values before the nose N_1 and the expected values after N_1 were used in an endeavour to compute $\lambda_3, \lambda_4 \ldots$ after the nose. But this did not succeed since convergence could not be reached in a reasonable amount of computer run time.

By observing that all the eigenvalues are negative in the single-solution range continued to the first nose N_1, we conclude that these steady-state solutions may be stable up to N_1. The other multiple solutions, existing past the first nose N_1 on the bifurcation diagram, have some eigenvalues associated with them that are positive and are thus unstable steady-state solutions. In terms of heat transfer coefficient at the wall [heat transfer at wall is proportional to $-\bar{\phi}(0)$], the result implies that of all multiple solutions at any R in the first family of solutions (near $R = 0$), only the one with the highest heat transfer coefficient at the wall may be stable, while others with lower heat transfer coefficients are unstable with time. The existence of multiple eigenvalues also lends support to the conjecture that there exist infinitely many noses in the bifurcation diagram and that corresponding to the ith nose N_i is an eigenvalue λ_i that changes sign (exactly once) from negative to positive at N_i as $\bar{f}(\infty)$ decreases.

For the second family of solutions (R near 0.5, see Figs. 3 and 4 for the bifurcation diagram) only one eigenvalue λ was found (Table 3). It changes sign at the nose N of the bifurcation curve indicating that only one of the steady-state solutions at each R may be stable, the one with the higher heat transfer coefficient at the wall. We conjecture (from Fig. 8) that the single eigenvalue λ for this second family of solutions decreases to 0 as $-\bar{\phi}'(0)$ decreases to 0 and R approaches 0.5 as well on the bifurcation curve.

The above eigenvalues were found to be reasonably insensitive to changes in c^*x (see Table 4). We remark that it is no accident that the eigenvalues, considered as functions of $[\bar{f}(\infty), R]$ or $[-\bar{\phi}'(0), R]$, change their signs independently of the value of x ($x > 0$). This is so because for $c^*x > 0$ the condition $c^*x\lambda = 0$ implies, for example, that $\lambda[\bar{f}(\infty), R] = 0$, and vice versa.

Thus our results establish that only one of the multiple steady states previously found may be stable with time, and one may expect to observe the corresponding flows experimentally. All the rest of the steady states are not stable with time, and thus one may not expect to observe any of the corresponding flows experimentally.

REFERENCES

1. B. Gebhart, B. Hassard, S. P. Hastings and N. D. Kazarinoff, Multiple steady-state solutions for buoyancy induced transport in porous media saturated with cold

Table 3. The third and further eigenvalues for solutions near $R = 0$

	R†	λ_3	λ_4	λ_5	λ_6	λ_7	λ_8	λ_9
	0.000000	-0.29120×10^{-1}	-0.38898×10^{-1}	-0.51034×10^{-1}	-0.65422×10^{-1}	-0.82018×10^{-1}	-0.10085×10^{-1}	-0.14559×10^{-1}
	0.050000	-0.20980×10^{-1}	-0.27629×10^{-1}	-0.35947×10^{-1}	-0.45875×10^{-1}	-0.70325×10^{-1}	-0.84843×10^{-1}	-0.10094×10^{-1}
a‡	0.100000	-0.17221×10^{-1}	-0.23892×10^{-1}	-0.32222×10^{-1}	-0.42124×10^{-1}	-0.66484×10^{-1}	-0.80954×10^{-1}	-0.97014×10^{-1}
b	0.125000	-0.15317×10^{-1}	-0.22014×10^{-1}	-0.30353×10^{-1}	-0.40244×10^{-1}	-0.64549×10^{-1}	-0.78992×10^{-1}	-0.95031×10^{-1}
c	0.155000	-0.87632×10^{-2}	-0.12432×10^{-1}	-0.74311×10^{-2}	-0.28988×10^{-1}	-0.44363×10^{-1}	-0.63117×10^{-1}	-0.73784×10^{-1}
d	0.180000	-0.38592×10^{-2}	-0.54320×10^{-2}	-0.74311×10^{-2}	-0.98424×10^{-2}	-0.12657×10^{-2}	-0.15868×10^{-1}	-0.23458×10^{-1}
	0.189296	-0.23472×10^{-2}	-0.34971×10^{-2}	-0.49561×10^{-2}	-0.67166×10^{-2}	-0.87738×10^{-2}	-0.11123×10^{-1}	-0.13763×10^{-1}
e	0.192446	-0.17051×10^{-2}	-0.27057×10^{-2}	-0.39735×10^{-2}	-0.55038×10^{-2}	-0.72921×10^{-2}	-0.93358×10^{-2}	-0.11632×10^{-1}
	0.192813	-0.14775×10^{-2}	-0.23511×10^{-2}	-0.34598×10^{-2}	-0.47995×10^{-2}	-0.63662×10^{-2}	-0.81577×10^{-2}	-0.10172×10^{-1}

† Please see Table 1 for corresponding values of $f(\infty)$ and η_{sc}.
‡ This point is identified by this alphabet on the accompanying figures. (All computations done at $c^*x = 10$.)

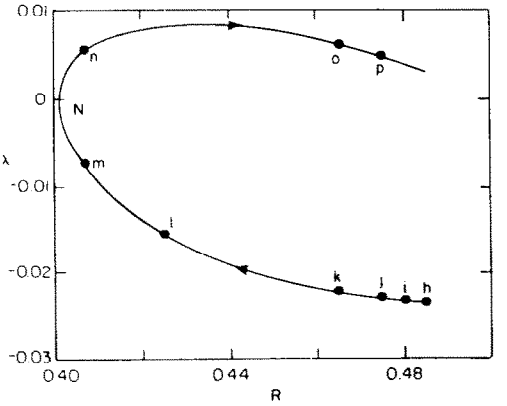

FIG. 8. The single eigenvalue λ for the family of solutions near $R = 0.5$.

pure or saline water, *Numer. Heat Transfer* **6**, 337–352 (1983).
2. C. P. Knowles and B. Gebhart, The stability of the laminar natural convection boundary layer, *J. Fluid Mech.* **34**, 657–686 (1968).
3. C. A. Heiber and B. Gebhart, Stability of vertical natural convection boundary layers: some numerical solutions, *J. Fluid Mech.* **48**, 625–646 (1971).
4. S. P. Hastings and N. D. Kazarinoff, On the bifurcation diagram for a problem in buoyancy induced flow, *Contemp. Math.* **17**, 395–400 (1983).
5. S. P. Hastings and N. D. Kazarinoff, Multiple solutions for a problem in buoyancy induced flow, *Archs ration. Mech. Analysis* **87**, 229–249 (1985).
6. I. El-Henawy, B. Hassard and N. D. Kazarinoff, A stability analysis of nontime-periodic perturbations of buoyancy induced flows in pure water near 4°C, *J. Fluid Mech.* **163**, 1–20 (1986).
7. Y.-K. Hwang, The stability of some multiple steady states and the effect of motion pressure in vertical natural convection flows in cold water. Ph.D. dissertation, SUNY, Buffalo (1984).
8. I. El-Henawy, B. Hassard, N. D. Kazarinoff, B. Gebhart and J. C. Mollendorf, Numerically computed multiple steady states of vertical buoyancy-induced flows in cold pure water, *J. Fluid Mech.* **122**, 235–250 (1982).
9. J. F. Brady, Flow development in a porous channel and tube, *Phys. Fluids* **27**, 1061–1067 (1984).
10. J. M. Ramilson and B. Gebhart, Buoyancy induced transport in porous media saturated with pure or saline water at low temperatures, *Int. J. Heat Mass Transfer* **23**, 1521–1530 (1980).
11. E. R. Lapwood, Convection of a fluid in a porous medium, *Proc. Camb. Phil. Soc.* **44**, 508–521 (1948).
12. R. A. Wooding, Steady state free thermal convection of a liquid in a saturated permeable medium, *J. Fluid Mech.* **2**, 273–285 (1957).
13. J. L. Beck, Convection in a box of porous material saturated with fluid, *Phys. Fluids* **15**, 1377–1383 (1972).
14. S. A. Bories and M. A. Combarnous, Natural convection in a sloping layer, *J. Fluid Mech.* **57**, 63–67 (1973).
15. B. Gebhart and J. C. Mollendorf, A new density relation for pure and saline water, *Deep Sea Res.* **24**, 813–848 (1977).
16. R. Burlisch and J. Stoer, Numerical treatment of ordinary differential equations by extrapolation methods, *Numerische Math.* **8**, 1–13 (1966).
17. P. Deuflhard, Recent advances in multiple shooting techniques. In *Computational Techniques for O.D.E.*

Table 4. The variation of the eigenvalue with c^*x near $R = 0.5$

		c^*x			
R	$-\bar{\phi}'(0)$	50.0	120.0	200.0	η_∞
0.480000	0.301769	-0.23509×10^{-1}	-0.14004×10^{-1}	-0.11427×10^{-1}	28
0.400825	0.100000	-0.40167×10^{-4}	-0.16766×10^{-4}	-0.10065×10^{-4}	40
0.404360	0.065000	0.88566×10^{-3}	0.36974×10^{-3}	0.22196×10^{-3}	40
0.420000	0.0292305	0.15969×10^{-2}	0.66661×10^{-3}	0.40018×10^{-3}	40
0.465000	0.0015545	0.12608×10^{-2}	0.52610×10^{-3}	0.31579×10^{-3}	52

(Edited by Caldwell and Sawyer), pp. 217–282. Academic Press, New York (1980).
18. P. Deuflhard and G. Bader, Multiple shooting techniques revisited, *Preprint* No. 163, Inst. für Angewandte Math., U. Heidelberg (1982).
19. U. Ascher, J. Christiansen and R. D. Russell, COLSYS—A collection code for boundary problems. In *Notes on Computer Science* (Edited by Goos and Hartmanis), No. 76, *Codes for Boundary-Value Problems in Ordinary Differential Equations*, pp. 164–185. Springer-Verlag, Berlin (1978).

APPENDIX: TRADITIONAL FORMULATION FOR HYDRODYNAMIC STABILITY

The conventional method of studying hydrodynamic stability of the system under consideration is outlined in this Appendix. It is shown that such a formulation (based on the analysis presented in refs. [2, 3]) leads to a singular coefficient in the governing equations. It is also demonstrated that the singularity can be eliminated by assuming the x derivatives of the time-dependent velocities to be small as compared to the y derivatives; and that the stability equations used in the previous sections may be extracted from the resulting equations.

First, the pressure terms are eliminated from the time dependent equations (3) by cross differentiation. After 'lumping' the constants together with the help of equations (10) and (21), the resulting equations are linearized about the steady-state solutions $\bar{u}(x, y)$, $\bar{v}(x, y)$ and $\bar{T}(x, y)$ by considering solutions of the form

$$u(x, y, t) = \bar{u}(x, y) + \varepsilon\hat{u}(x, y, t) + O(\varepsilon^2) \quad \text{(A1a)}$$

$$v(x, y, t) = \bar{v}(x, y) + \varepsilon\hat{v}(x, y, t) + O(\varepsilon^2) \quad \text{(A1b)}$$

$$T(x, y, t) = \bar{T}(x, y) + \varepsilon\hat{T}(x, y, t) + O(\varepsilon^2) \quad \text{(A1c)}$$

where ε is small and positive. Neglecting the change in $\bar{u}$, $\bar{v}$ and $\bar{T}$ with respect to x, as compared to those with respect to y, dividing through by ε and taking limits as $\varepsilon \to 0$, and cancelling out the steady-state terms with the help of equations (7), the resulting equations yield

$$\frac{1}{c}\frac{\partial}{\partial t}\left[\frac{\partial\hat{u}}{\partial y} - \frac{\partial\hat{v}}{\partial x}\right] + \left[\frac{\partial\hat{u}}{\partial y} - \frac{\partial\hat{v}}{\partial x}\right] = \pm q\frac{\alpha_1 c_1^2}{2}\frac{\operatorname{sign}(\bar{T} - T_m)}{|T_0 - T_\infty|^q}\frac{\partial}{\partial y}[|\bar{T} - T_m|^{q-1}\hat{T}] \quad \text{(A2a)}$$

$$\frac{(\rho C_p)_{er}}{(\rho C_p)_{fr}}\frac{\partial\hat{T}}{\partial t} + \bar{u}\frac{\partial\hat{T}}{\partial x} + \hat{u}\frac{\partial\bar{T}}{\partial x} + \bar{v}\frac{\partial\hat{T}}{\partial y} + \hat{v}\frac{\partial\bar{T}}{\partial y} = \alpha_1\left[\frac{\partial^2\hat{T}}{\partial x^2} + \frac{\partial^2\hat{T}}{\partial y^2}\right]. \quad \text{(A2b)}$$

The plus/minus sign corresponds the coordinate system in Figs. 2a/2b, respectively.

The final form of the equations after substituting the mathematical forms of perturbations $\hat{u}$, $\hat{v}$ and $\hat{T}$ is not presented here since the object is to demonstrate that a singularity is introduced in the coefficients of the linear stability equation and that it can be removed. The singularity exists on the RHS of equation (A2a) since $1 < q < 2$, i.e. $|\bar{T} - T_m|^{q-2}$ (obtained after simplifying $\partial/\partial y$) is singular at $\bar{T} = T_m$.

This singular behaviour may be eliminated only if, in addition to neglecting the change in steady-state physical quantities with respect to x as compared to changes with respect to y, we also assume that the change in the time-dependent velocity perturbations $\hat{u}$ and $\hat{v}$ with respect to x can be neglected as compared to those with respect to y (as done in Section 2). Then equation (A2a) may be integrated to yield [after using the boundary condition at $y = \infty$, equation (5)]

$$\frac{1}{c}\frac{\partial\hat{u}}{\partial t} + \hat{u} = \pm q\frac{\alpha_1 c_1^2}{2}\frac{\operatorname{sign}(\bar{T} - T_m)}{|T_0 - T_\infty|^q}|\bar{T} - T_m|^{q-1}\hat{T}. \quad \text{(A3)}$$

We define (see discussions in refs. [2, 3])

$$\psi(x, y, t) = \bar{\psi}(x, y) + \varepsilon\hat{\psi}(x, y, t) + O(\varepsilon^2) \quad \text{(A4)}$$

$$\hat{\psi}(x, y, t) = \alpha_1(Ra_x)^{1/2}\tilde{f}(\eta)e^{i(ax - \beta t)} \quad \text{(A5a)}$$

$$\hat{T}(x, y, t) = (T_0 - T_\infty)\tilde{\phi}(\eta)e^{i(ax - \beta t)} \quad \text{(A5b)}$$

where η is the similarity variable defined by equation (9). Here $\mathrm{Re}(a)$ is the wave number in the x direction ($= 2\pi$ divided by wavelength), and $\mathrm{Re}(\beta)$ is the angular frequency ($= 2\pi$ multiplied by frequency). (Note that a and β are complex numbers independent of x.) If $\mathrm{Im}(\alpha) < 0$ the wave will amplify with increasing x, while if $\mathrm{Im}(\beta) > 0$ the wave will amplify with time. For the case $\mathrm{Im}(\alpha) = \mathrm{Im}(\beta) = 0$, the wave will be neutrally stable and will neither amplify nor decay.

From equations (11), (A4), (A5) and using the derivatives of the perturbation stream function $\hat{\psi}$ to represent $\hat{u}$ and $\hat{v}$, equations (A3) and (A2b) are transformed to (for $0 \leqslant \eta \leqslant \infty$)

$$-i\beta^*\frac{d\tilde{f}(\eta)}{d\eta} + \frac{d\tilde{f}(\eta)}{d\eta} = \pm q\operatorname{sign}[\tilde{\phi}(\eta) - R]\,|\tilde{\phi}(\eta) - R|^{q-1}\tilde{\phi}(\eta) \quad \text{(A6a)}$$

$$-i\beta^* c^* x\tilde{\phi}(\eta) - \left[\tilde{f}(\eta)\frac{d\tilde{\phi}(\eta)}{d\eta} + \tilde{f}(\eta)\frac{d\tilde{\phi}(\eta)}{d\eta}\right] + i2ax\left[\tilde{\phi}(\eta)\frac{d\tilde{f}(\eta)}{d\eta} - \tilde{f}(\eta)\frac{d\tilde{\phi}(\eta)}{d\eta}\right] = \frac{d^2\tilde{\phi}(\eta)}{d\eta^2} + \frac{1}{Ra_x}\left[\eta^2\frac{d^2\tilde{\phi}(\eta)}{d\eta^2} + 3\eta\frac{d\tilde{\phi}(\eta)}{d\eta} - 4a^2x^2\tilde{\phi}(\eta) - i4ax\eta\frac{d\tilde{\phi}(\eta)}{d\eta}\right]. \quad \text{(A6b)}$$

where equation (21) defines c^* and

$$\beta^* = \beta/c. \quad \text{(A7)}$$

The boundary conditions are given by equations (26). Equations (A6) and (26) form the stability-eigenvalue problem.

We make the following remarks.

1. If the change in $\hat{T}$ with respect to x is neglected when compared to the changes with respect to y (the large Ra_x case), the RHS of equation (A6a) becomes

$$\frac{d^2\tilde{\phi}(\eta)}{d\eta^2}. \quad \text{(A8)}$$

2. If $a = 0$ and $\beta = i\mathrm{Im}(\beta)$ (i.e. $-i\beta^* = \lambda$, λ real) then the system of equations (A6b) and (A8) reduces to the system (25) and (26) studied in Section 2.
3. The system (A6) is equivalent to a sixth-order system of differential equations with real-valued dependent variables. The system of linear stability equations studied in Section 2 is order three, which results in a significant simplification in the numerical analysis. Further, the x dependence of the coefficients in equations (A6) is more complicated than the x dependence in the system (25) and (26) in Section 2.
4. The singularity which occurs in deriving the classical linear stability equations can be avoided by not eliminating the pressure terms [6]. This approach was not adopted because it introduces additional pressure variables and adds to the complexity of the mathematical system of equations, reducing the efficiency of computations.

STABILITE DE LA CONVECTION NATURELLE AVEC EXTREMUM DE DENSITE DANS UN MILIEU POREUX

Résumé—On étudie la stabilité relative d'états multiples de convection libre laminaire dans un milieu poreux saturé avec l'eau pure froide, le long d'une surface plane, verticale et isotherme. On trouve dans la bibliographie deux régions distinctes de solutions numériques d'états d'équilibre multiples pour des conditions d'écoulements dans lesquels le domaine de température couvre un maximum de densité ($0 < R < 1/2$, où R est un paramètre de rapport de température). L'analyse de stabilité de ces états d'équilibre est conduite en linéarisant les équations dépendant du temps autour des solutions d'état permanent et en considérant seulement l'amplification ou l'amortissement des perturbations dans le temps. Les résultats obtenus montrent que tous les états multiples d'équilibre, sauf un, à chaque R sont instables vis-à-vis du temps. On discute l'approche utilisée dans cette étude par rapport à l'analyse de stabilité hydrodynamique conventionnelle.

STABILITÄT EINER FREIEN KONVEKTIONSSTRÖMUNG IN DER UMGEBUNG EINES DICHTE-EXTREMUMS IN EINEM PORÖSEN MEDIUM

Zusammenfassung—Es wurde die relative Stabilität der verschiedenen stationären Zustände von laminaren freien Konvektionsströmungen entlang einer vertikalen isothermen und ebenen Oberfläche in einem porösen mit kaltem, reinem Wasser gesättigten Medium untersucht. Von zwei unterschiedlichen Bereichen numerisch berechneter Lösungen mit verschiedenen stationären Zuständen für die Strömungsbedingungen, bei welchen der Temperaturbereich ein Dichte-Extremum ($0 < R < 1/2$ mit R als Temperaturverhältnis) beinhaltet, wird in der Literatur berichtet. Die Stabilität dieser stationären Zustände wurde durch Linearisierung der zeitabhängigen Gleichungen um die stationären Lösungen und die alleinige Betrachtung von Verstärkung oder Abschwächung der Störungen über die Zeit untersucht. Die so ermittelten Ergebnisse zeigen, daß alle (bis auf einen) verschiedenen stationären Zustände bei jedem R im Hinblick auf die Zeit instabil sind. Jeweilige Vorzüge und Mängel des Näherungsverfahrens in dieser Untersuchung gegenüber der konventionellen hydrodynamischen Stabilitätsanalyse wurden erörtert.

УСТОЙЧИВОСТЬ СВОБОДНОКОНВЕКТИВНОГО ТЕЧЕНИЯ В ПОРИСТОЙ СРЕДЕ ПРИ НАЛИЧИИ ЭКСТРЕМУМА ПЛОТНОСТИ

Аннотация—Исследуется относительная устойчивость множества стационарных состояний ламинарных свободноконвективных потоков в пористом материале, насыщенном холодной чистой водой, вдоль вертикальной, изотермической плоской поверхности. В опубликованных работах отмечалось наличие двух отчетливых областей в численных стационарных решениях для таких условий течения, при которых внутренний диапазон температур включает максимум плотности ($0 < R < 1/2$, где R—параметр, учитывающий отношение температур). Проведен анализ устойчивости стационарных состояний линеаризацией нестационарных условий относительно стационарных решений и рассматривая только усиление или ослабление возмущений во времени. Полученные результаты показывают, что за исключением одного все стационарные состояния для каждого значения R являются неустойчивыми во времени. Рассмотрены преимущества и недостатки используемого метода по сравнению с обычным анализом гидродинамической устойчивости.